C. R. Acad. Sci. Paris, t. 2, Série IV, p. 1139–1151, 2001
Physique appliquée/*Applied physics*
(Biophysique/*Biophysics*)

IMAGERIE ACOUSTIQUE ET OPTIQUE DES MILIEUX BIOLOGIQUES
OPTICAL AND ACOUSTICAL IMAGING OF BIOLOGICAL MEDIA

Tissue harmonic ultrasonic imaging

Michalakis A. AVERKIOU

ATL Ultrasound, PO Box 3003, Bothell, WA, 98041-3003, USA
E-mail: mike.averkiou@philips.com

(Reçu le 10 juillet 2001, accepté le 28 juillet 2001)

Abstract. Harmonic imaging was originally developed for microbubble contrast agents in the early 90s under the assumption that tissue is linear and all harmonic echoes are generated by the bubbles. In fact, tissue, like bubbles, is a nonlinear medium. Whereas the harmonic echoes from bubbles have their origins in nonlinear scattering, those from tissue are a result of nonlinear propagation. The clinical benefits of tissue harmonic imaging are reduced reverberation noise and overall clutter level, improved border delineation, increased contrast resolution, and reduced phase aberration artifacts. To a large extent these benefits are explained by the properties of nonlinear propagation of the transmitted ultrasonic pulses in the tissue. © 2001 Académie des sciences/Éditions scientifiques et médicales Elsevier SAS

imaging / ultrasound / nonlinear / harmonic / acoustics / constrat agent perfusion

Imagerie ultrasonore harmonique des tissus

Résumé. *L'imagerie ultrasonore harmonique a d'abord été développé pour suivre les agents de contraste formés de microbulles dans les années 90, en faisant l'hypothèse que la propagation dans les tissus était linéaire et que les harmoniques n'étaient générées que par les bulles. En fait les tissus ont aussi un comportement non linéaire. Alors que les échos harmoniques des bulles proviennent de la diffusion non linéaire, ceux des tissus proviennent des propriétés de propagation non linéaire. L'intérêt de l'imagerie harmonique, sur le plan clinique est de réduire le bruit de réverbération, d'améliorer les contours des organes, d'augmenter la résolution et de réduire certaines aberrations. Ces différentes améliorations s'expliquent par les propriétés de la propagation non linéaire des ultrasons dans les tissus. © 2001 Académie des sciences/Éditions scientifiques et médicales Elsevier SAS*

imagerie / ultrasons / non lineaire / harmonique / acoustique / agent de contraste / perfusion

1. Introduction

Tissue Harmonic Imaging (THI) was introduced in 1997 [1] and is today routinely used in diagnostic ultrasound imaging. Some of the problems encountered in diagnostic imaging are blood flow measurement in the microcirculation (at the capillary level), tough acoustic windows that result in reverberation artifacts, passage through inhomogeneous layers that cause phase aberration and beam distortion, and contrast resolution. Microbubble contrast agents were introduced in the early 90s to address only the first problem mentioned above, i.e., blood perfusion. Contrast agents are gas filled microbubbles with typical diameters

Note présentée par Guy LAVAL.

S1296-2147(01)01259-8/FLA

of a few microns that are injected into the blood. They oscillate under sonification, thus increasing the backscattered signals and enhancing the ultrasonic images. The nonlinear nature of bubble dynamics lends itself to harmonic imaging, a procedure by which energy is being transmitted in a fundamental frequency f and an image is formed with the backscattered signals at the second harmonic $2f$. One of the first assumptions in attempting harmonic imaging of contrast agents was that tissue is linear, and thus only the contrast microbubbles in the blood would produce second harmonic signals. The harmonic images observed before contrast microbubble injection were at first believed to be the result of transmitted second harmonic energy directly from the transducer, or incomplete rejection of the fundamental during the filtering process. It was soon discovered that the harmonic images before injection of contrast agents was the result of a nonlinear process in tissue.

The discovery of harmonic imaging was found to help in all the traditional diagnostic imaging problems mentioned above. In all areas of diagnostic imaging — cardiology, radiology, peripheral vascular — harmonic imaging offered improvements over conventional (fundamental) imaging in certain patient populations and imaging conditions [2]. That lead to increased research activity in nonlinear tissue imaging. The first observation was that the harmonic echoes from bubbles have their origins in nonlinear scattering and those from tissue are a result of nonlinear propagation and subsequent linear scattering. For contrast applications the tissue harmonic component is noise for the bubble harmonic signals.

The field of nonlinear acoustics is well established and a variety of texts and papers exists in literature [3]. Nonlinear propagation of sound (both plane waves and sound beams) has been studied in a number of investigations. As early as 1980 it has been suggested in the literature that biomedical frequencies and intensities cause nonlinear acoustical effects [4,5]. Further investigation on nonlinear effects in tissue followed the introduction of contrast agents and the observation of harmonic imaging's advantages over conventional imaging [6,7].

In this paper, first the clinical benefits of THI are reviewed and demonstrated with images. The main clinical issues are presented as well as some of the considerations in diagnostic imaging. A brief review of nonlinear propagation of sound beams follows. The roles of absorption, medium nonlinearity, and diffraction in nonlinear propagation are explained. A series of simulations illustrate the nonlinear acoustic field produced in tissue from both circular and rectangular transducers. The pulse distortion due to the nonlinear propagation is observed at various depths and propagation curves and beam patterns for the fundamental and second harmonic component are shown. The pulse inversion and pulse-to-pulse amplitude modulation techniques are demonstrated. Finally, all of the above properties of nonlinear acoustics are used to explain the clinical benefits of THI and give physical insight to its properties.

2. Clinical benefits and issues of THI

Harmonic imaging is the formation of an ultrasound image from the backscattered signal at twice the frequency of the sonification signal. In microbubble contrast applications the harmonic components are generated by the nonlinear scattering from bubbles. In THI the harmonic components are generated during the nonlinear propagation of sound in tissue. In this section the benefits of THI are shown first and in a later section are related to certain properties of nonlinear propagation.

2.1. Reverberations from tough acoustic windows

In cardiology the heart is imaged through the ribs and lungs. The acoustic window (entry plane) plays an important role on the resulting image. In conventional imaging very often the image is noisy and shows repeated artifacts thoughout its depth (see *figure 1a*). Since the acoustic beam has to fit between the ribs and avoid the lungs, part of the beam may actually be obstructed and reflected back. These reflections are often reflected back in the body again after reflecting from the transducer and they register as coming from a deeper region. As seen in *figure 1a* the clutter is making the myocardium very difficult to assess. In *figure 1b* harmonic imaging is used and the clutter level is dramatically reduced producing a clearer image

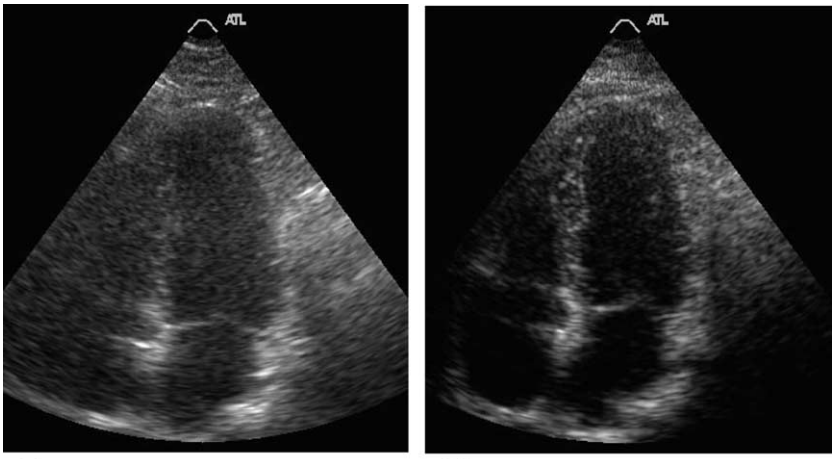

Figure 1. A cardiac image showing a 4-chamber view of the heart in fundamental imaging (a), and harmonic imaging (b). Reverberation artifacts are seen through the image as clutter and 'haze' in (a), and they are absent in the harmonic image (b).

of the heart muscle. Apparently, the harmonic beam suffers lees than the fundamental from the passage through the acoustic window.

2.2. Phase aberration from inhomogeneous layers

Diagnostic imaging systems usually assume a constant speed of sound $c_0 = 1540$ m/s and density $\rho_0 = 990$ kg/cm. However, the various tissues along the imaging path have different impedances $z = c_0\rho_0$. After all, if it was not for the different impedance along the image path we would not have an image. Even within the same kind of tissues there are still variations in the speed of sound. This results in an effective defocusing of the beam and the resulting images are 'hazy'. In abdominal imaging where the beam has to go through layers of fat, muscle, and other layered tissues and membranes this artifact is often encountered and clutter and 'haze' throughout the image is present (see *figure 2a*). The 'haze' in the aorta (the diagonal darker area in the lower part of the image) is not generated at that depth but in the shallow part of the image where the beam has to go through layers of tissue and fat. The effective defocusing of the beam resulted in the clutter seen in *figure 2a*. In *figure 2b* however, the aorta is cleaner. For reasons explained in later sections, it seems that the harmonic beam is not as defocused as the fundamental one.

2.3. Endocardial visualization and border delineation

Both of the problems discussed above also result in reduced boarder delineation. The endocardial boarders are not clearly differentiated in the presence of noise. The same applies for the abdominal image. Harmonic imaging greatly reduces the problem. Interfaces and boundaries tend to be more difficult to identify in fundamental versus harmonic imaging (compare *figure 3a* and *b*). The apex (top section) and lateral wall (right side) of the heart muscle are not seen in *figure 3a* because it is buried under noise but in *figure 3b* those regions are clearly seen. Also in *figure 2b* the boarder between the liver and other tissues and structures is better delineated than in *figure 2a*.

2.4. Problems of THI

It has often been observed that the THI images have reduced axial resolution, especially in the early days of harmonic imaging. The transducer-beamformer bandwidth limits the overall axial resolution of harmonic

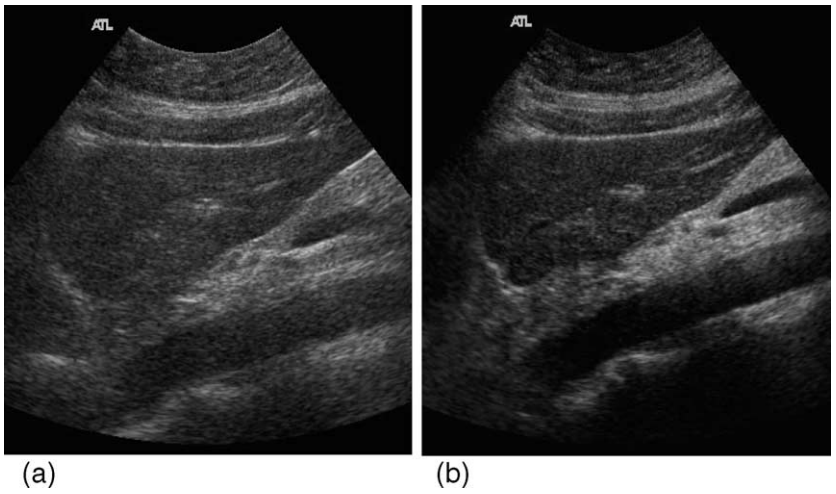

Figure 2. An abdominal image showing the liver and aorta in conventional (fundamental) imaging (a), and harmonic imaging (b). Phase aberration artifacts due to inhomogeneities in the tissue layers are seen as noise in the fundamental image especially inside the aorta.

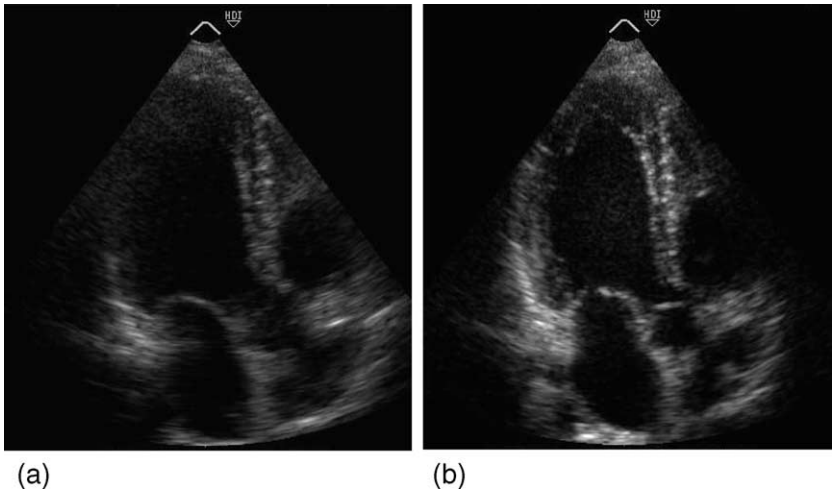

Figure 3. A cardiac image showing a 4-chamber view of the heart in conventional (fundamental) imaging (a), and harmonic imaging (b). In harmonic imaging the endocardial boarders are better seen.

images. In conventional imaging the total bandwidth of the transducer is used for best resolution. However, in harmonic imaging both the transmit and receive bandwidths must fit within the total bandwidth of the transducer. This forces the use of a lower and narrower transmit bandwidth which results in reduced axial resolution. Another reason for reduced axial resolution is the requirement that the harmonic bandwidth be separable from the transmit, so conventional radio-frequency (RF) filters may be able to reject the fundamental components. This problem is solved with pulse inversion as discussed later.

Other problems encountered in THI is reduced dynamic range and penetration. Since the image is formed with only the second harmonic component which is usually at least 20 dB below the fundamental the dynamic range is limited. Furthermore, the overall second harmonic energy generated (usually 10% of the original fundamental or less) is absorption limited in deep regions.

3. Theory

In nonlinear acoustics, the propagation speed of a wave, c, is not constant as is assumed in linear acoustics (e.g., $c_0 = 1540$ m/s), but it is a function of the particle velocity due to the wave disturbance, $c = c_0 + \beta u$, where u is the particle velocity and $\beta = 1 + B/(2A)$ is the coefficient of nonlinearity of the medium [3]. Thus, the positive peak of the wave where the particle velocity is high has a faster propagation speed than the negative peak of the wave where the particle velocity is low. This variation of the propagation speed results in a waveform distortion also referred to as wave 'steepening' which shifts energy from the fundamental to the higher harmonic components. Another important parameter in diagnostic imaging is the absorption due to the thermoviscous losses, as the sound propagates in tissue energy is lost in the form of thermoviscous absorption. In the high frequency imaging applications this is more prominent since the absorption is proportional to the frequency. The medium absorption becomes the limiting factor in the maximum depth that may be imaged. Finally, a third property of sound fields that is very relevant in imaging is diffraction which relates to the collimated nature of the sound field as well as the focusing properties.

The combined effects of diffraction, absorption, and nonlinearity in directive sound beams are modeled by the KZK nonlinear parabolic wave equation [8]. The KZK equation is solved via a numerical code in dimensionless form. We introduce four normalized variables, $P = p/p_0$, $\sigma = z/d$, $\rho = r/a$, $\tau = \omega_0 t'$ and $t' = t - z/c_0$ the retarded time, where p and p_0 is the sound and source pressure respectively, z the coordinate along the axis of the beam, r is the transverse radial coordinate, d the focal length, a the aperture radius, and ω_0 a characteristic angular frequency. The KZK equation becomes [9]:

$$\frac{\partial P}{\partial \sigma} = \frac{1}{4G}\int_{-\infty}^{\tau}\left(\frac{\partial^2 P}{\partial \rho^2} + \frac{1}{\rho}\frac{\partial P}{\partial \rho}\right)\mathrm{d}\tau' + A\frac{\partial^2 P}{\partial \tau^2} + N\frac{\partial P^2}{\partial \tau} \tag{1}$$

The first term (integral) on the right-hand side of equation (1) accounts for diffraction. The second term accounts for thermoviscous dissipation of sound which includes losses due to shear viscosity, bulk viscosity, and heat conduction. The third term accounts for quadratic nonlinearity of the fluid. The three dimensionless parameters that describe the relative importance of diffraction, absorption and nonlinearity are:

$$G = z_0/d, \qquad A = \alpha_0 d, \qquad N = d/\overline{z} \tag{2}$$

respectively. The first parameter, G is the small-signal focusing gain, where $z_0 = \omega_0 a^2/2c_0$ is the Rayleigh distance. In a linear lossless case the pressure at the focus is $P(\sigma = 1) = G$. The absorption parameter contains the thermoviscous attenuation coefficient $\alpha_0 = \delta\omega_0^2/2c_0^3$. In the nonlinearity parameter the term $\overline{z} = \rho_0 c_0^3/\beta\omega_0 p_0$ is the plane wave shock formation distance. The source condition appropriate for a uniform focused source is:

$$P = f\left(\tau + G\rho^2\right)H(1-\rho) \quad \text{at } \sigma = 0 \tag{3}$$

In general, equation (1) is an accurate model of the sound field produced by directive sound sources ($ka \gg 1$, where k is the wavenumber) at distances beyond a few source radii and in regions close to the axis of the source, the paraxial region (up to about 20° off the z axis in the farfield). These restrictions are satisfied in most practical applications of directive sound beams, including diagnostic ultrasound. The KZK equation has been used by many researchers and was found to be in excellent agreement with experiments [10,11].

Equation (1) was solved numerically in the time domain using finite-difference operators to approximate the derivatives. The algorithm used was similar to that given by Lee and Hamilton [9] for unfocused, diverging sound beams except that a rectangular grid was used to accommodate the geometry of focused beams.

Source functions $f(\tau)$ for equation (3) in the simulations used in this paper are generated with:

$$f(\tau) = \exp\left[-(\tau/N_c\pi)^{2m}\right],\ \sin[\tau + \phi] \tag{4}$$

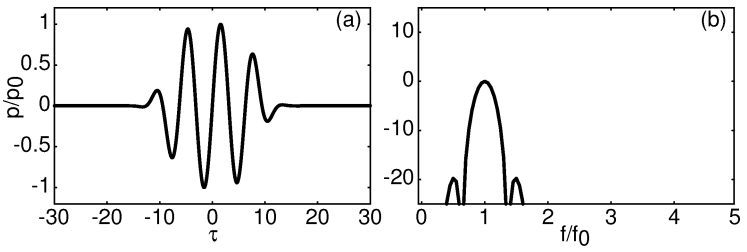

Figure 4. Source function for numerical simulations with $N_c = 3$ and $m = 2$. Time waveform (a), spectrum (b).

where m is proportional to the envelope slope and N_c is proportional to the number of cycles. In *figure 4*, equation (4) is used to generate a source function with $N_c = 3$, and $m = 2$.

In diagnostic ultrasound rectangular array transducers are used and not circular like equation (1) assumes. However, the physical properties of the sound beams remain in general the same. The reason that circular transducers were given more attention in the past in theoretical and numerical investigations is due to the reduced computation time to solve equation (1) due to the axisymmetric source condition that drastically reduces the computation points. With the increased computing power in today's computers a nonaxisymmetric form of the KZK equation may be solved numerically as well. The radial coordinate ρ is replaced by $\chi = x/a_x$, and $\psi = y/a_y$ where x, a_x, y, and a_y are the azimuthal and elevational coordinates and half–dimensions, respectively, i.e., the full source dimensions are $2a_x \times 2a_y$. The axial coordinate now becomes $\sigma = z/d_x$. The nonaxisymmetric form of the KZK equation is:

$$\frac{\partial P}{\partial \sigma} = \int_{-\infty}^{\tau} \left(\frac{1}{4G_x} \frac{\partial^2 P}{\partial \chi^2} + \frac{1}{4G_y} \frac{\partial^2 P}{\partial \psi^2} \right) \mathrm{d}\tau' + A \frac{\partial^2 P}{\partial \tau^2} + N \frac{\partial P^2}{\partial \tau} \tag{5}$$

where G_x and G_y is the focusing gain in the azimuthal and elevation direction, respectively. The source condition now becomes:

$$P = f\left(\tau + G_x \chi^2 + G_y \psi^2\right) H(1-\chi) H(1-\psi) \quad \text{at } \sigma = 0 \tag{6}$$

Equation (4) is still used to generate source functions in the simulations in the next section. Similar finite difference approaches used in solving the axisymmetric form of the KZK equation are used to numerically solve equation (5). The computation times are considerably larger due to the increased number of finite difference calculations required to solve the diffraction integral. The number of computation points is effectively squared.

The degree of nonlinearity in THI (the level of the second harmonic component) is proportional to the Mechanical Index (MI) which is displayed in diagnostic ultrasound systems as required by the FDA. The MI is defined as $MI = p_-/\sqrt{f}$, where p_- is the peak negative pressure measured in MPa and f is the frequency measured in MHz. Use of a higher MI in a diagnostic system promotes more nonlinear propagation and thus higher second harmonic.

4. Results

In this section numerical results are presented from simulations with the KZK equation. The majority of the simulations are for a circular focused source for simplicity and faster computation times but results from a rectangular nonaxisymmetric source are also presented. The results show certain attributes of the nonlinear field from sound beams and relate them with the properties and clinical benefits of THI.

The simulations are all for tissue under diagnostic ultrasound conditions and realistic THI parameters for cardiac imaging. The parameters used are $f = 1.55$ MHz, $c_0 = 1540$ m/s, $\rho_0 = 1000$ kg/m^3, $a = 10$ mm, $d = 80$ mm, $\beta = 5$, and $\alpha_0 = 5.35$ Np/m (equivalent to 0.3 dB/(cm·MHz), as the FDA requires for the regulatory measurements). The source radius was chosen such that its area would be the same as the area of the P4–2 phased array used for cardiac imaging, and the frequency and focal length are the default

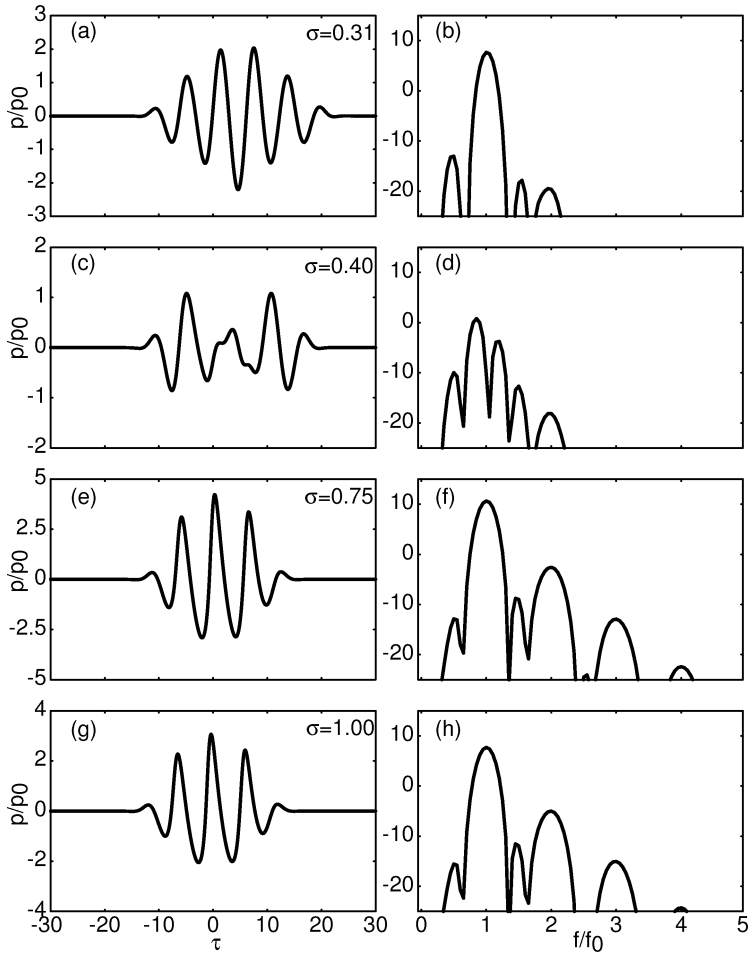

Figure 5. Time waveforms and their respective spectra along the axis of a focused source with $G = 3.95$, $A = 0.43$, $N = 0.48$.

values used for THI in the ATL HDI-5000. The source pressure amplitude is $p_0 = 0.45$ MPa and the source function is as shown in *figure 4*. This value of p_0 results in $MI = 1.2$, a typical value for THI. The focusing gain of this source condition is $G = 3.95$ and the absorption and nonlinearity parameters are $A = 0.43$ and $N = 0.48$. Time waveforms (pulse shapes) and their respective spectra at various depths are shown in *figure 5*.

In (a) the waveform very close to the transducer is shown and as seen in its spectrum (b) very little second harmonic is generated. The pulse shown in (c) is at an axial position where the field has a diffraction minimum. That is where the center wave and edge wave are out of phase [10]. In (e) we see the pulse at its maximum value even though it is still only at $\sigma = 0.75$. In the spectrum (f) the second harmonic is only 15 dB below the fundamental. At the focus (g) and beyond (not shown here) the beam starts to spread (the amplitude is reduced) but the second harmonic maintains a relatively large value.

The variation of the fundamental and the second harmonic components along the axis of the source is shown in *figure 6*. It is acquired by taking the FFT of the time waveform at every propagation step. In *figure 6a* the pressure is shown in a dB scale so that both the fundamental and the 2nd harmonic are seen in the same scale. In *figure 6b* the normalized pressures for the fundamental and second harmonic with respect to the on-axis maximum are shown. It should be noted that the second harmonic is roughly 25 or more dB below the fundamental up to $\sigma = 0.4$ but it increases and stays at a higher value around the focus and beyond. Another property of the harmonic component seen in *figure 6b* is that it reaches its maximum

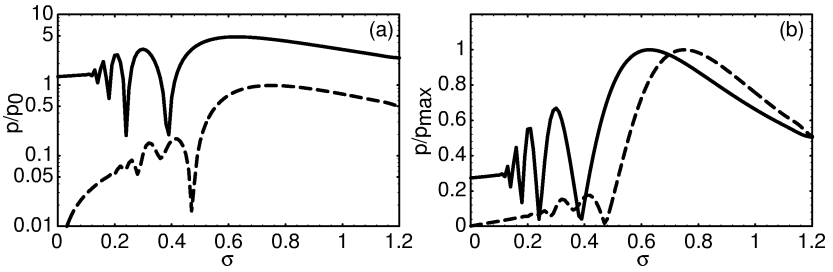

Figure 6. Propagation curve for fundamental and second harmonic along the axis of a focused source with $G = 3.95$, $A = 0.43$, $N = 0.48$ in dB (a), and in an absolute scale normalized with respect to the on-axis maximum (b).

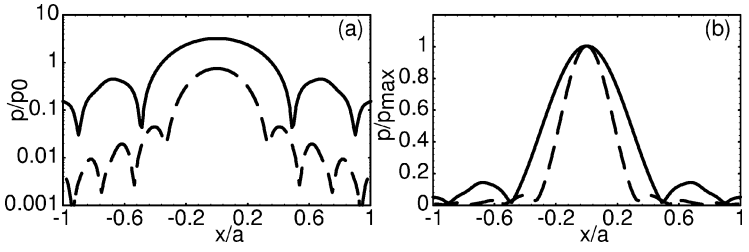

Figure 7. Beam patterns for fundamental and second harmonic at $\sigma = 1.0$ for a focused source with $G = 3.95$, $A = 0.43$, $N = 0.48$.

at a deeper range than the fundamental. This is due to its cumulative nature. It is always being generated by the fundamental around it from a region that is close to the source axis.

The variation of the fundamental and second harmonic component across the source axis (beam patterns) at $\sigma = 1.0$ is shown in *figure 7*. It is noted that the fundamental has sidelobes that are about 17 dB down the on-axis level but the second harmonic has sidelobes that are about 25 dB down. The reduction in the sidelobe level is due to the fact that the second harmonic is generated only around the source axis where the fundamental has its highest amplitude, from a virtual volume source. In *figure 7b* the normalized beampatterns are shown in absolute scale as well. A reduced sidelobe level is always a good property for the imaging beam. The sidelobes are often responsible for the clutter in the image.

4.1. Pulse inversion

The axial resolution limitation of harmonic imaging is overcome with a new imaging method called pulse inversion [12]. The pulse inversion technique consists of transmitting 2 or more of pulses with every new pulse being the inverse of the previous one (different in phase by π) and adding the echoes in such a way that the fundamental component is removed before any RF-filtering operation. This method removes the requirement of narrow band transmit for harmonic signal extraction and even in the case of broadband transmit where fundamental and harmonic components overlap the second harmonic component is isolated. Since the original pulses differ by π their respective odd harmonic components ($n = 1, 3, 5, \ldots$) differ by $n\pi$ and are inverses of one another and cancel by addition whereas the even harmonic components ($n = 2, 4, 6, \ldots$) double since they differ by $2n\pi$. In *figure 8* the pulse inversion technique is demonstrated. The two pulses at the source plane are shown in (a) and their spectrum in (b). In (c) the pulses at $\sigma = 0.75$ are shown. In (e) the sum of the two pulses in (c) is shown and its spectrum in (f). As seen in (f) only the even harmonic components are left after this process. Extension of this technique to more than 2 pulses addresses tissue motion.

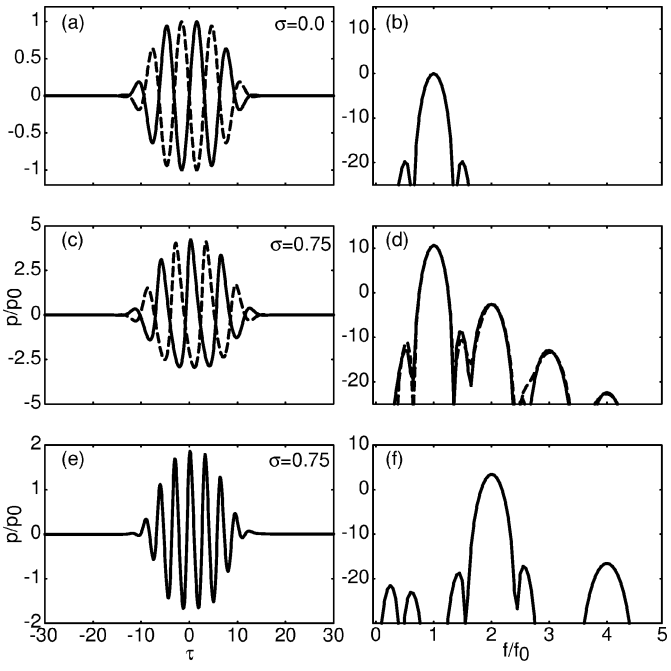

Figure 8. Pulse inversion technique. The pulses at the source plane (a) and their spectra (b). Pulses at $\sigma = 0.75$ (c), and their spectra (d). Sum of pulses at $\sigma = 0.75$ (e), and its spectrum (f).

4.2. Pulse-to-pulse amplitude modulation

Another technique that isolates the nonlinear components is the pulse-to-pulse amplitude modulation. This technique consists of transmitting 2 or more pulses at different amplitudes and adding the echoes from these pulses by scaling with the inverse of the factor used in transmit. Here we consider the case where they differ by a factor of 4 (the second one is $1/4$ the first) as well by π in phase (see *figure 9a* and *b*). The

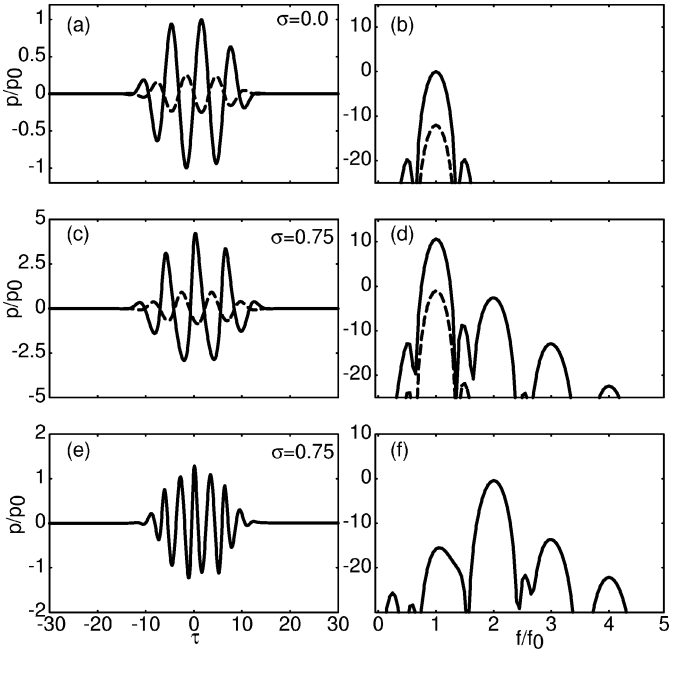

Figure 9. Pulse-to-pulse amplitude modulation technique. The pulses at source plane (a), and their spectra (b). Pulses at $\sigma = 0.75$ (c). Sum of pulses in (b) according to $e_1 + 4e_2$ (c) and its spectrum (f).

returned echoes are added according to $e_1 + 4e_2$, where e_1 and e_2 are the returned echoes from the first (solid line in (3)) and second pulse (dashed line in (3)), respectively. This technique relies in comparing the nonlinear activity at different amplitudes. In the limiting case where the second pulse is very low such that no nonlinear propagation takes place, by scaling it and adding to the first pulse all of the linear fundamental component is removed. This method, like the pulse inversion method, allows broad-band nonlinear imaging and may be used with more than 2 pulses to address motion problems.

4.3. The nonlinear field of a rectangular phased array

In this section results from the numerical solution of equation (5) are shown. They simulate the field of a P4–2 phased array used on an HDI-5000. The source dimensions and medium parameters are as follows: $a_x = 10.08$ mm, $a_y = 13$ mm, $d_x = 100$ mm, $d_y = 81$ mm, $G_x = 3.21$, $G_y = 1.65$, $A = 0.53$, $N = 0.60$, and the same source function as the one used for the circular source shown in *figure 4* was used. The maximum mechanical index for this case is $MI = 1.02$. As suggested earlier the same trends with the circular source are seen where the second harmonic component is low close to the source and increases around the focus. This is better demonstrated with the propagation curves of *figure 10*. Most of the problems in diagnostic imaging usually originate at the superficial tissue layers where the second harmonic has not fully developed yet. In *figure 11* the transverse field at $\sigma = 1.0$ for the fundamental and second harmonic component is shown. The first sidelobe for the fundamental is 13 dB down from the on-axis value and for the second harmonic is 19 dB down. Considering the degree of agreement between experimental measurements and numerical results from the KZK found in the literature, the simulations in *figures 10* and *11* are expected to be a very realistic description of the acoustic field in tissue.

In order to get a better visualization of the fundamental and harmonic field of the P4–2 in a tissue-like medium, contour plots of the field are shown in *figure 12*. The diffraction pattern of the fundamental beam (*figure 12a*) shows the nearfield oscillations, the sidelobes at the focus, as well as farfield variations. The second harmonic contour plot (*figure 12b*) shows a much smoother field which would be better suited for imaging purposes. The second harmonic field at a specific range is generated from the existing fundamental beam at that same range as well as before that range. However, only the regions of the fundamental beam that have a considerable high amplitude generate a second harmonic. Those regions are located only at the center of the beam. All the ripples of the fundamental beam (in *figure 12b*) are of a lower amplitude and thus do not contribute much in the second harmonic field.

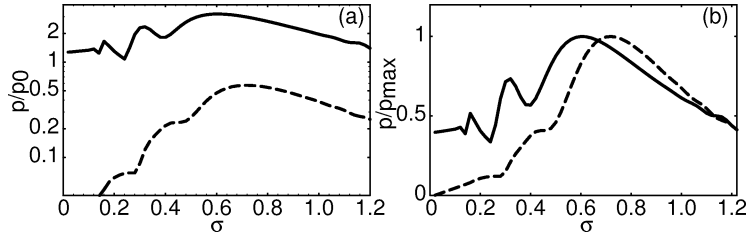

Figure 10. Propagation curve for fundamental and second harmonic for the P4–2 phased array with $G_x = 3.21$, $G_y = 1.65$, $A = 0.53$, and $N = 0.60$.

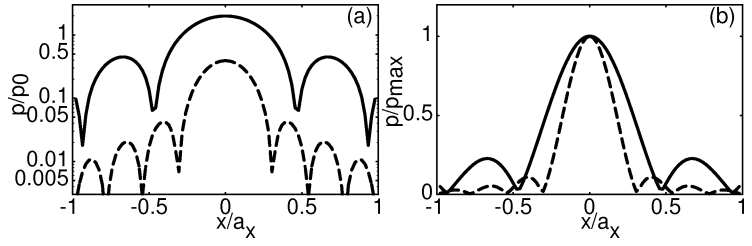

Figure 11. Beam patterns for fundamental and second harmonic for the P4–2 phased array with $G_x = 3.21$, $G_y = 1.65$, $A = 0.53$, and $N = 0.60$.

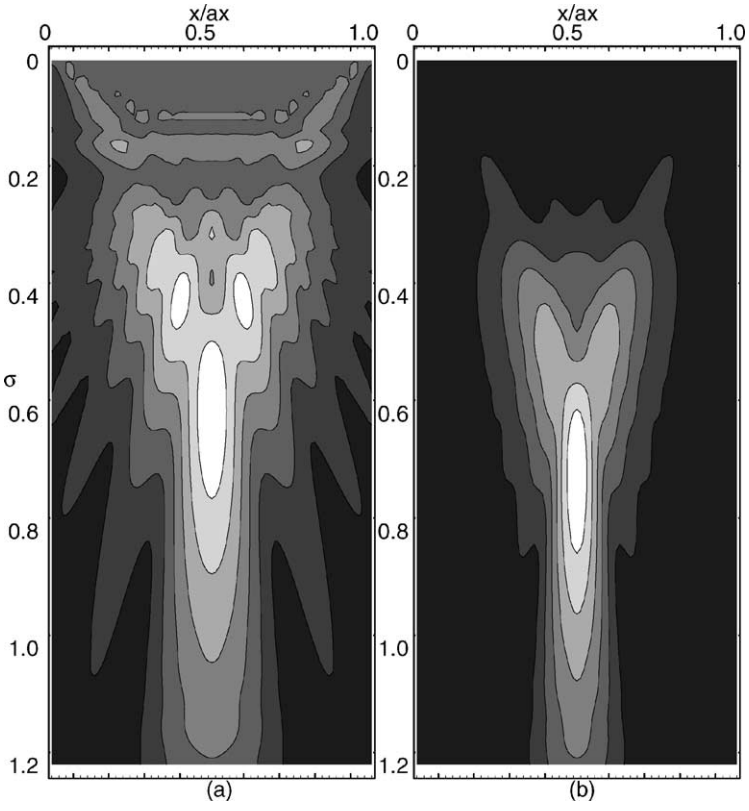

Figure 12. Contour plots for fundamental and second harmonic for the P4–2 phased array with $G_x = 3.21$, $G_y = 1.65$, $A = 0.53$, and $N = 0.60$.

5. Discussion

As exhibited by the images in this paper and as suggested by the literature, the second harmonic beam suffers considerably less than the fundamental in propagating through tissue. As a simple demonstration, here we consider the case where 10% of the transmitted energy is reflected at an interface close to the transducer surface and after a subsequent reflection at the transducer it re-propagates into the tissue. We call the first beam the 'main' beam and the reflected beam the 'clutter' beam. A simulation is shown in *figure 13* that corresponds to the above situation. The clutter beam fundamental is about 20 dB below the main beam fundamental as assumed in this scenario. However, the clutter beam second harmonic which is generated by the considerably reduced clutter fundamental is about 40 dB below the main second harmonic. This simplified scenario indicates how multiple reverberations from passage through a tough window or an

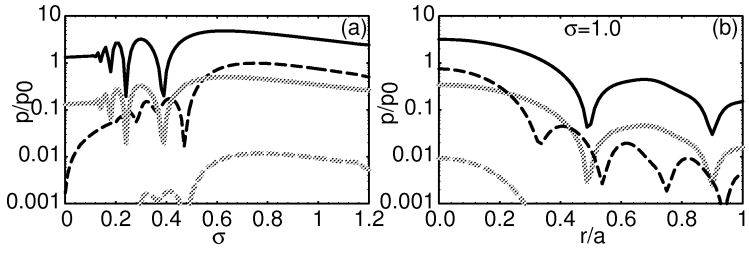

Figure 13. Reflection of 10% of the main beam. Solid lines indicate the main fundamental and dashed lines the main second harmonic. The lighter gray solid and dashed lines indicate the clutter beam. Propagation curves in (a) and beam patterns in (b).

aberrating layer greatly affect the fundamental beam but not as much the second harmonic. The same characteristics are seen in the transverse field in *figure 13b*.

As seen in earlier sections, nonlinear propagation of sound waves from focused beams in tissue has some interesting properties that contribute to the characteristics of tissue harmonic images. The fundamental beam is generated at the transducer whereas the harmonic beam is generated continuously along the propagation path as a consequence of the local instantaneous amplitude. The harmonic beam can be considered as a volume source that starts at the transducer and extends out to the point of interest. Because it has double the frequency, the harmonic beam is narrower than the fundamental. Its sidelobes, responsible for degradation of image contrast, are lower than those of the fundamental as shown in *figure 11* for a phased array transducer. These properties result in increased lateral resolution, reduction of the multiple reflections due to a poor acoustic window, and overall clutter reduction. Inhomogeneities of the speed of sound in superficial tissue layers cause phase aberration in the fundamental beam, distorting the resulting image. The harmonic beam is not fully generated until the focus and beyond and consequently suffers less from aberration in superficial tissue. The clutter energy is low enough and it does not generate harmonic components. This explains the reduction of noise in abdominal images and the improved border delineation in echocardiography.

6. Conclusion

Nonlinear propagation in tissue is responsible for the harmonic echoes that are used to form THI images. The lower sidelobes of the second harmonic component result in reduced clutter in the image. In the nearfield where the tough acoustic windows and aberrating tissue layers are encountered, trapped reflected echoes are produced. Those echoes are largely fundamental and avoided by forming an image with only the second harmonic component. The reduced axial resolution in harmonic imaging due to the transducer bandwidth is overcome by the pulse inversion technique. A limitation of this technique is that only even harmonic components are detected. This limitation may be overcome by a similar technique that uses noninteger-π shifts [13]. Pulse-to-pulse amplitude modulation may also be used to isolate the nonlinear energy and allow broader bandwidths. Even though THI was discovered accidently in an effort to image bubble echoes while assuming that tissue is linear, the clinical accomplishments of THI thus far have been tremendous. Further research on nonlinear propagation of sound beams in tissue-like (inhomogeneous, aberrating) media should offer more clinical benefits.

References

[1] Averkiou M.A., Roundhill D.R., Powers J.E., A new imaging technique based on the nonlinear properties of tissues, in: Proc. IEEE Ultrason. Symp., Vol. 2, 1997, pp. 1561–1566.
[2] Becher H., Tiemann K., Pohl C., Nanda N.C., Averkiou M.A., Powers J.E., Luderitz B., Improvement in endocardial border delineation using tissue harmonic imaging, Echocardiography 15 (1998) 511–517.
[3] Hamilton M.F., Blackstock D.T., Nonlinear Acoustics, Academic Press, San Diego, CA, 1998.
[4] Muir T.G., Carstensen E.L., Prediction of nonlinear acoustic effects at biomedical frequencies and intensities, Ultrasound Med. Biol. 6 (1980) 345–357.
[5] Carstensen E.L., Law W.K., McKay N.D., Muir T.G., Demonstration of nonlinear acoustical effects at biomedical frequencies and intensities, Ultrasound Med. Biol. 6 (1980) 359–368.
[6] Ward B., Baker A.C., Humphrey V.F., Nonlinear propagation applied to the improvement of resolution in diagnostic medical imaging, J. Acoust. Soc. Am. 101 (1) (1997) 143–147.
[7] Christopher T., Finite amplitude distortion-based inhomogeneous pulse echo ultrasonic imaging, IEEE Trans. Ultrason. Ferr. Freq. Control 44 (1997) 125–139.
[8] Bakhvalov N.S., Zhileikin Ya.M., Zabolotskaya E.A., Nonlinear Theory of Sound Beams, American Institude of Physics, New York, 1987.
[9] Lee Y.S., Hamilton M.F., Time-domain modeling of pulsed finite-amplitude sound beams, J. Acoust. Soc. Am. 97 (1995) 906–917.

[10] Averkiou M.A., Hamilton M.F., Nonlinear distortion of short pulses radiated by plane and focused circular pistons, J. Acoust. Soc. Am. 102 (5) (1997) 2539–2548.
[11] Baker A.C., Berg A.M., Tjøtta J.N., The nonlinear pressure field of plane, rectangular apertures: Experimental and theoretical results, J. Acoust. Soc. Am. 97 (1997) 3510–3517.
[12] Hope Simpson D., Chin C.T., Burns P.N., Pulse inversion doppler: A new method for detecting nonlinear echoes from microbubble contrast agents, IEEE Trans. Ultrason. Ferr. Freq. Control 46 (2) (1999) 372–382.
[13] Bruce M.F., Averkiou M.A., Skyba D.M., Powers J.E., A generalization of pulse inversion doppler, in: Proc. IEEE Ultrason. Symp., 2000.